HIGH INTENSITY EFFECTS IN THE SNS ACCUMULATOR RING*

J.A. Holmes, S. Cousineau, V. Danilov, M.A. Plum, A. Shishlo, ORNL, Oak Ridge, TN 37830, U.S.A.

Abstract

Currently operating at 0.5 MW beam power on target, the Spallation Neutron Source (SNS) is already the world's most powerful pulsed neutron source. However, we are only one third of the way to full power. As we ramp toward full power, the control of the beam and beam loss in the ring will be critical. In addition to practical considerations, such as choice of operating point, painting scheme, RF bunching, and beam scattering, it may be necessary to understand and mitigate collective effects due to space charge, impedances, and electron clouds. At each stage of the power ramp-up, we use all available resources to understand and to minimize beam losses. From the standpoint of beam dynamics, the losses observed so far under normal operating conditions have not involved collective phenomena. We are now entering the intensity regime in which this may change. In dedicated high intensity beam studies, we have already observed resistive wall, extraction kicker impedance-driven, and electron cloud activities. The analysis and simulation of this data are important ongoing activities at SNS. This paper discusses the status of this work, as well as other considerations necessary to the successful full power operation of SNS.

INTRODUCTION

With production beam power now exceeding 0.5 MW and accumulated production beam intensities of ~0.6×10^{14} protons per pulse, SNS is now on the threshold of high intensity operation. To reach this point, much work has gone into the basic understanding of the machine and into mitigating the many problems encountered. In the ring, steering and tune selection algorithms have been developed. Basic lattice parameters and tunes have been measured. Cross plane coupling and chromaticity have been measured and corrected. Characterization of the collimation system has begun. Simulation and benchmarking between experiment and the Online Model [1] and the ORBIT Code [2] have been done at low intensities. Substantial amounts of work and design correction have gone into the injection chicane and injection dump line [3], which failed as originally installed to perform according to specification. Even now, the injection region is the most complicated and least understood area of the ring.

In a high intensity machine such as SNS, the most important requirements are good beam control and low beam loss. These are intimately related since low beam loss is required for good beam control. In addition to satisfying loss constraints, good beam control entails the satisfaction of beam distribution and intensity requirements at the target, at the stripper foils, and in various dumps and windows. These latter aspects of beam control require optimized painting schemes and transport from source to target. In this paper, we concentrate on the issue of losses in the ring. Low beam loss is one of the defining requirements of a high intensity accelerator. In SNS, the required overall fractional beam loss is 1.0×10^{-3} and the uncontrolled fractional beam loss requirement is 1.0×10^{-4}. These unprecedented low fractional losses are necessary to permit timely maintenance and high availability. Beam loss in SNS is caused by beam halo. We define beam halo to mean all beam that falls outside its intended range in 6D phase space. Halo in SNS has many possible causes, including upstream problems, such as bad or partial chopping; foil scattering in the injection region; single particle effects, due to resonances and to magnet alignment and field errors; collective effects from space charge and impedances; and electron cloud effects. Some of these causes of halo, such as bad chopping, foil scattering, and single particle effects, are present at all intensities, but only become concerns at high intensities where the absolute sizes of the associated losses become large. On the other hand, halo generation due to collective effects and electron clouds only occurs at high intensity. In this paper we illustrate the occurrence and analysis of several of these halo-generating, loss-causing mechanisms in the SNS ring.

BAD OR PARTIAL BEAM CHOPPING

Bad or partial chopping can lead to beam loss in the ring. Beam chopping occurs at low energy in the Low Energy Beam Transport (LEBT) and Medium Energy Beam Transport (MEBT) sections before the linac. Bad chopping can lead to beam-in-gap and, consequently, to high losses at extraction. When the choppers are performing properly, this doe not occur. Partial chopping increases the transverse emittance of the linac beam, thus increasing the quantity of H^- beam that misses the stripper foil and which must then undergo transport to the injection dump. We will not elaborate on halo generation due to beam chopping here, but losses in the injection dump are studied in the next section.

INJECTION DUMP BEAM LOSS

Thus far, the injection region and dump line (Fig. 1) have suffered the highest losses in SNS. Beam loss has been particularly high in the injection dump line, and much work has been done to correct this situation [3]. The measures already taken have caused losses to move downstream in the line, and it is now believed that scattering from the secondary stripper foil is a major

* ORNL/SNS is managed by UT-Battelle, LLC, for the U.S. Department of Energy under contract DE-AC05-00OR22725.

contributor. The purpose of the secondary foil is to strip all unstripped H^- or partially stripped H^0 beam after the primary stripper foil so that these waste beams can be directed to the injection dump.

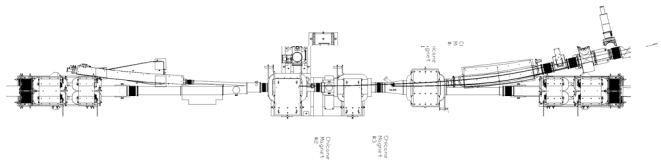

Figure 1. SNS ring injection area.

The carbon secondary stripper foil in place until now is 18 mg/cm^2 thick, which leads to abundant scattering. However, a foil thickness of just 1 mg/cm^2 is sufficient to completely strip the waste beams. It is structurally difficult to fabricate a thin foil because the area of the secondary stripper foil must be substantial in order to intercept both the H^- and H^0 waste beam components. In order ascertain the contribution of scattering in the secondary stripper foil to losses in the injection dump line, we compared losses with stripper foil in place to those with the secondary foil viewscreen replacing the stripper foil. The secondary foil viewscreen consists of Al2O3 of thickness 1 mm.

We compared the losses using three approaches: a simple analytic Rutherford scattering model [4], ORBIT Code [2] simulations, and experimental measurements, alternatively with the foil and with the viewscreen in place. Geometric considerations suggest that beam that is scattered between $6 \rightarrow 10$ mr at the secondary stripper foil will be lost in the injection dump line. Scattering angles greater than 10 mr will not clear the injection dump septum, while beam scattered by less than 6 mr can reach the dump.

Figure 2 compares the distributions of particles scattered by the secondary stripper foil and by the secondary foil viewscreen for 10^6 incident particles and three scattering models: multiple Coulomb scattering [4], Rutherford scattering [4], and the ORBIT scattering model [2]. The ORBIT model includes contributions from multiple Coulomb scattering, Rutherford scattering, elastic nuclear scattering, and inelastic nuclear reactions. The ORBIT model agrees closely with the multiple Coulomb scattering model at the small angles for which multiple Coulomb scattering is dominant, and with the Rutherford scattering model at the intermediate angles where it dominates. At large angles, where nuclear elastic scattering dominates, ORBIT predicts more scattered particles than do Rutherford or multiple Coulomb scattering. ORBIT oversimplifies nuclear inelastic scattering by removing these particles from the distribution.

By analyzing the scattering predictions in the range from $6 \rightarrow 10$ mr, we find that the Rutherford scattering model predicts 38 times as much scattering loss when the viewscreen is in place as for the secondary stripper foil. Similarly, the ORBIT model predicts a ratio of 35 for viewscreen scattering loss divided by foil scattering loss. Assuming a constant non-scattering-related loss in the injection dump, we can compare observed losses with the secondary foil and the viewscreen to determine the fraction of overall beam loss due to scattering. This has been carried out for two cases: a single waste beam to the injection dump tuned for minimum overall losses, and a simulated H^0 beam component to the injection dump. It was not possible to carry out the test for the H^- waste beam because this component does not impact the secondary foil viewscreen. Comparison of the beam loss monitor readings for these two cases shows a loss ratio of approximately 50 throughout the injection dump line for the optimized beam and a decreasing ratio ranging from 40→15 moving down the beam line for the simulated H^0 waste beam. For these cases, the predictions are essentially 100% beam loss due to scattering in the optimized case and from 90%→30% beam loss as a function of position along the beam line due to scattering for the simulated H^0 beam. In response to this situation, a new thinner 3.2 mg/cm^2 secondary stripper foil has been fabricated and installed, and we anticipate injection dump losses to reduce accordingly during the next run.

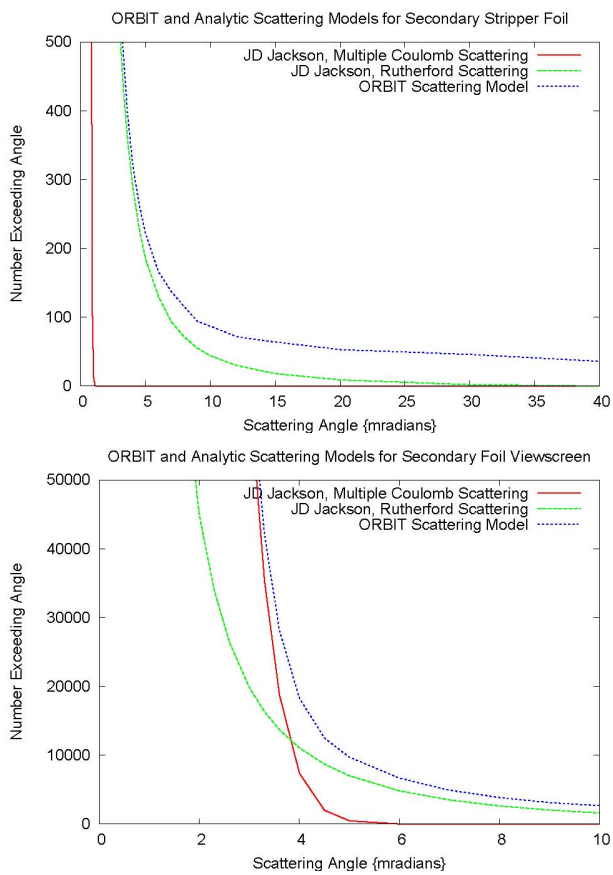

Figure 2. Scattering angle distributions in secondary stripper foil (top) and secondary foil viewscreen (bottom) for analytic multiple Coulomb scattering (red), Rutherford scattering (green), and ORBIT (blue) models.

LATTICE RESONANCES

Resonances can cause halo growth and beam loss, although in SNS with only ~1000 turns of accumulation, we expect only low order resonances to contribute significantly. The effects and correction of sextupole and octupole resonances in the SNS ring have been studied computationally by Fedotov, Parzen, and coworkers [5]. In their work, which included space charge forces, it was found that resonances occur when collective, not individual particle, modes are excited by the lattice imperfections. Their simulations show that these resonances lead to a significant enhancement of the beam tail, but that most of this undesirable beam growth can be removed through resonance correction, which they carried out using the sextupole and dipole correctors to reduce the appropriate islands observed in single particle tracking. Thus, they found that correcting the single particle resonance stopband was sufficient to significantly reduce the beam growth with space charge present. Their calculations were carried out for working points in the vicinity $(Q_x, Q_y) = (6.40, 6.30)$, but we typically operate SNS at $(Q_x, Q_y) = (6.23, 6.20)$, which was selected to avoid low order lattice resonances. Thus, in the millisecond accumulation times of the SNS ring we don't experience halo generation due to lattice resonances.

ALIGNMENT AND FIELD ERRORS

Magnet alignment and field errors introduce closed orbit and betatron phase distortions and x-y coupling. Their effect and correction was studied for many cases of randomly introduced errors using ORBIT [6]. The SNS ring lattice, including BPMs and dipole and quadrupole correctors, was simulated for single turn injection with errors present. The dipole and quadrupole correctors were then activated to correct the closed orbit distortions and phase advances using a least squares algorithm. The correction was carried out alternatively both with and without BPM signal errors. The uncorrected and corrected lattices were then simulated for otherwise identical full intensity injection scenarios of 1.44 MW and 1060 turns. In order to tabulate losses, a complete set of apertures was included in the calculations. In tests over many cases, the correction procedure proved successful. In some cases, without correction, more than 20% of the beam is lost. With correction, and assuming exact BPM signals, fractional beam loss is less than $2*10^{-4}$. Finally, with correction and assuming BPM signal errors, fractional beam loss is still less than $3*10^{-4}$. ORBIT simulations conclude that the SNS ring orbit correction system using BPM signals to optimize dipole corrector and quadrupole family strengths is adequate to correct orbit deviations, phase advances, and losses for alignment and field errors at the anticipated levels. Similar optimization techniques have been implemented for closed orbit correction in the SNS application software [1] and are applied routinely to set the ring dipole corrector magnets. Activation of the trim quadrupoles for phase correction is yet to be carried out.

The correction of x-y coupling in the ring has also been carried out, using the formalism of Sagan and Rubin [7]. Coupling in the ring could complicate delivery of the desired beam distribution to the target. Transverse coupling was measured by injecting a single turn with a large vertical offset and small horizontal offset relative to the closed orbit. The correction procedure reduced the observed coupling by a factor of five, with the coupling coefficient decreasing from 0.22→0.046 and the maximum horizontal amplitudes at a typical selected BPM decreasing from 17 mm to 3.5 mm. The resulting x-y coupling is sufficiently small to provide satisfactory control of the beam distribution.

INJECTION REGION LOSSES

Beam losses are high in the ring on the downstream side of the injection region. Contributing to this situation is the fact that the beam pipe narrows upstream of the injection kickers, which are used for painting the transverse distribution. Consequently, the beam is off center at the aperture restriction.

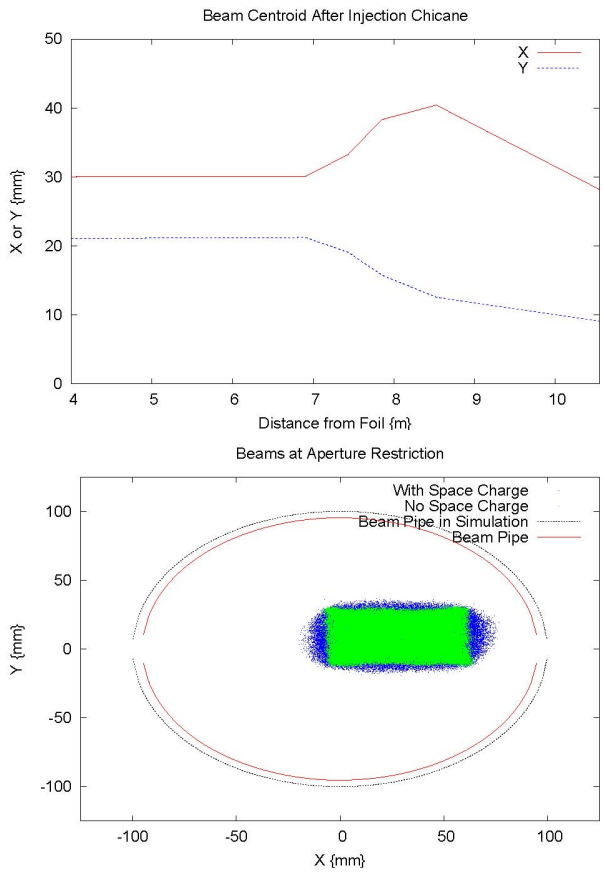

Figure 3. Horizontal and vertical beam centroids in the high loss injection region (top). Beam footprints at the aperture restriction in the high loss injection region.

Scattering in the primary stripper foil is suspected to contribute significantly to the observed losses. The primary foil is quite thin, consisting of carbon and having an approximate thickness of 300 μg/cm^2. The ORBIT

scattering model predicts that fractional losses due to inelastic nuclear scattering in the primary foil are on the order of 2×10^{-6} per foil hit. Injection simulations of accumulation at full intensity in SNS result in 6 to 15 foil hits per proton, depending on the painting scheme.

Another contributing factor may be space charge, which is known to broaden high intensity beam distributions [8, 9]. We study the relative contributions of foil scattering and space charge to injection region losses using ORBIT simulations. Again, we include a complete set of apertures around the ring in order to tabulate losses. We consider full intensity accumulation of 1.5×10^{14} protons over 1060 turns at 1 GeV, which corresponds to 1.44 MW beam power. The calculations are carried out in three ways: with space charge and foil scattering; with space charge but no foil scattering, and finally without space charge or foil scattering. Figure 3 shows the beam centroids (top) tracked through the high loss section of the injection region from the end of the final chicane dipole to the start of the first injection kicker following injection. The horizontal axis shows the distance downstream from the primary stripper foil measured in meters and the aperture restriction occurs just upstream of the upper limit. The centroid values change as the beam passes through the quadrupole doublet. The horizontal and vertical beam centroid displacements off center at the aperture restriction are about 30 mm and 10 mm, respectively. The second plot of Fig. 3 (bottom) shows the beam footprint at the aperture restriction for cases with (blue) and without (green) space charge. The effect of space charge in broadening the beam is clearly visible.

We now present numerical results of a typical ORBIT simulation. The chosen painting scheme resulted in about 15.2 foil hits/proton, which is consistent with estimates for schemes used at present. Total fractional loss with space charge and foil scattering was 4.0×10^{-3}, compared with 2.7×10^{-3} with foil scattering turned off. From this we estimate that total fractional losses due to foil scattering are 1.3×10^{-3}. Total losses with both space charge and foil scattering turned off were zero, so in this case the 2.7×10^{-3} total fractional beam loss can be attributed to space charge. Most of this loss occurs as controlled beam loss in the collimation section of the ring. If we restrict our attention to uncontrolled losses, most are in the high loss injection region. The results here are 1.3×10^{-4} total fractional loss with space charge and foil scattering, 0.5×10^{-4} fractional beam loss due to space charge, and 0.8×10^{-4} due to foil scattering. Of the injection region loss due to foil scattering, about half (0.4×10^{-4}) is due to inelastic nuclear reactions. The work presented here is still in progress. As shown in the bottom plot of Fig. 3, the aperture at the beam pipe narrowing used in the calculations was taken to be 100 mm, but in referring to detailed drawings we learned that the actual limiting aperture is a bellows with a radius of 95.25 mm. In addition to repeating the calculation for this aperture, we must consider various painting schemes and RF waveforms to optimize the losses. However, these results suggest that optimized transverse and longitudinal painting schemes that keep foil hits at a minimum and also minimize beam broadening due to space charge will be very important in satisfying loss constraints in the SNS ring.

COLLECTIVE INSTABILITIES

Although we have yet to observe instabilities under normal operating conditions, we have seen instabilities during dedicated high intensity studies [10, 11]. In these studies we have now accumulated up to 1.3×10^{14} protons without instability. However, we have observed instabilities by removing stabilizing conditions. This was done by lowering the RF voltage to produce coasting, instead of bunched, beams; by correcting the chromaticity to give zero, rather than natural, chromaticity; and by storing the beam for thousands of turns without extraction. We have barely begun the analysis of these observations.

The dominant impedance in the SNS ring is due to the extraction kickers, and previous calculations [12] indicate that this could lead to instability in the 4→10 MHz range at high intensities. This instability is most likely to occur for coasting beams and zero chromaticity. As reported in Ref. [10], the extraction kicker instability has been observed under these conditions for a range of intensities above about 3μC (~2×10^{13} protons). The tune settings for these observations were (Q_x, Q_y) = (6.23, 6.21).

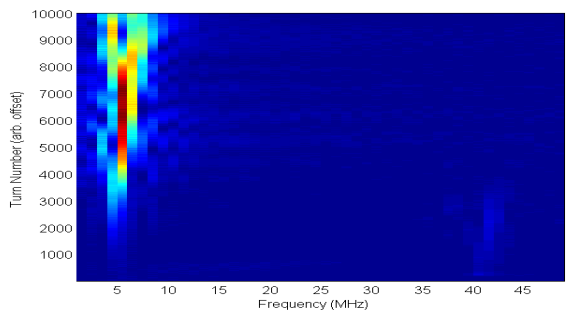

Figure 4. Turn-by-turn frequency spectrum of the coasting beam extraction-kicker-induced instability seen in SNS.

Figure 4 shows a waterfall plot of the vertical spectrum evolution of the instability over 10000 turns at 12μC beam intensity. This transverse instability is dominant in the vertical direction, although there is some horizontal activity due to x-y coupling. The dominant harmonic is at 6 MHz and there is noticeable excitation in the 4→10 MHz range for a stored coasting beam. Interpreting this to be a "slow" mode, the frequency is consistent with dominant harmonic n = 12, and excitation in the range $10 \le n \le 16$. The observed growth rate of this instability was used to estimate the extraction kicker impedance, with the result of 28 kΩ/m, which is in excellent with the predicted value of 22→30 kΩ/m. We are in the process of simulating this instability using the ORBIT code, and although we haven't done the simulation for the exact parameters of this case, we have carried out a coasting beam calculation for a case with natural chromaticity and

a higher intensity of 1.1×10^{14} protons (~17.6μC). The results, shown in Fig. 5, show significant activity in the harmonics n = 10→16 (which correspond to frequencies of 4→10 MHz) with n = 14 as the dominant harmonic. The overall peak-to-peak beam distortions are sizeable at more than 25 mm. In order to obtain a quantitative comparison with the experiment, we intend to repeat the calculation using 12μC and zero chromaticity.

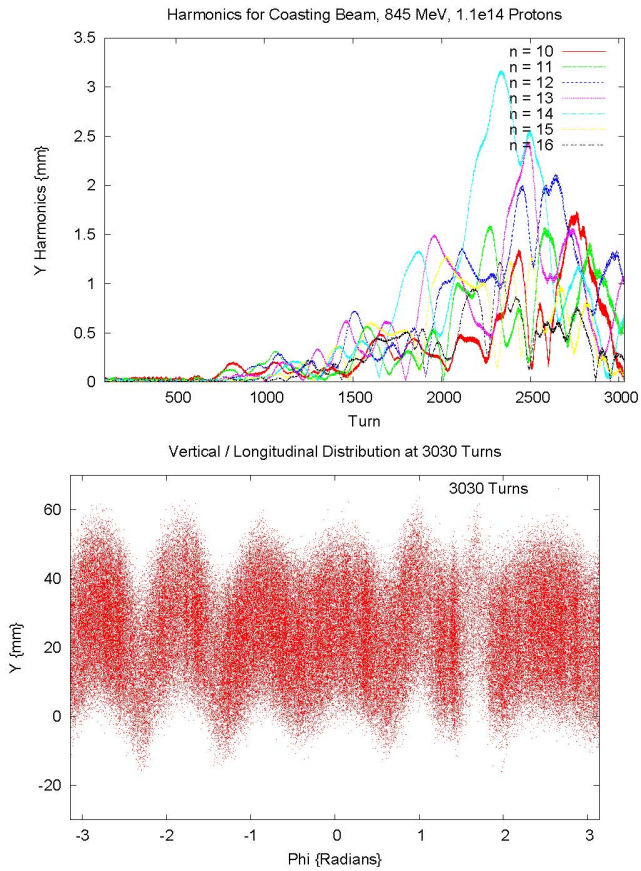

Figure 5. Extraction kicker impedance instability simulation: evolution of harmonics n = 10→16 (top). Vertical beam distribution versus longitudinal position at 3030 turns.

Another impedance-driven instability observed in SNS is the resistive wall instability, which occurs when the operating tunes are set below integer values. This observation was reported in detail in Ref. [10]. In the experiment the ring was tuned to $(Q_x, Q_y) = (5.795, 5.8)$, in order to produce an instability in the regime of high impedance. The expected instability frequency was 200 kHz, and a narrow band instability was observed at 191 kHz, consistent with tunes of 5.81. The growth rate of the instability was used to calculate a resistive wall impedance of 34 kΩ/m, which is consistent with estimated values. We have not yet simulated this case.

The electron cloud instability has been observed in all the dedicated high intensity studies to date. The electron cloud instability initially develops toward the first half of the proton beam and extends toward the rear as the instability grows. Analysis of experimental BPM data for coasting beams places the onsets of instability at 3.4×10^{13} protons in the horizontal plane and at 5.8×10^{13} protons vertically. However, higher intensities are obtained in the vertical direction. We are now performing self-consistent simulations of some of these cases, but these are expensive calculations in terms of computer resources, and the work proceeds slowly. Thus far, we have only one completed calculation using experimental operating parameters. Figure 6 shows the turn-by-turn vertical frequency spectrum of a coasting beam e-p instability in SNS. The top plot shows measured results and the bottom shows the results of an ORBIT simulation [13]. The range and extent of the simulation frequency spectrum are lower and smaller than the experimental spectrum. Both the measured and the simulated spectra drift toward lower frequencies as the instability evolves. Although the simulation agrees qualitatively with reality, there are quantitative differences. These may be due to the position and localization of the electron cloud nodes in the simulations.

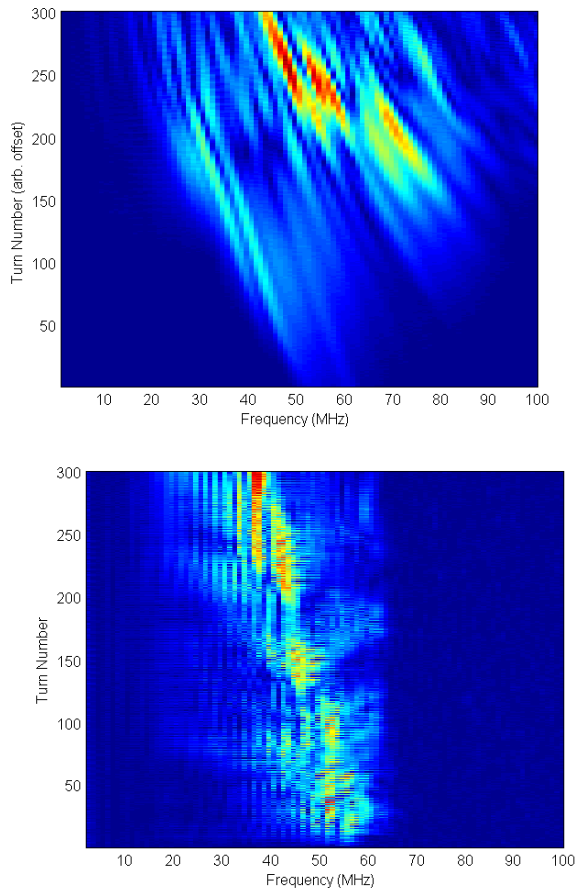

Figure 6. Turn-by-turn vertical frequency spectrum of the coasting beam e-p instability seen in SNS. Top: measured results. Bottom: ORBIT simulation.

CONCLUSIONS

We have reached the threshold of high intensity in the SNS ring: ~0.6×10^{14} protons accumulated in production

and ~1.3×10^{14} protons accumulated in dedicated studies. Our main concern as we ramp to higher power is beam loss caused by halo. We are studying and evaluating the causes and effects of halo-generating mechanisms including foil scattering, resonances and magnet errors, space charge, collective instabilities, and the e-p instability. As we enter the high intensity regime, we expect our primary emphasis to shift from concerns such as foil scattering to collective phenomena and electron clouds. In these areas, we are just getting started.

REFERENCES

[1] J. Galambos, "SNS Application Programming," http://neutrons.ornl.gov/APGroup/appProg/appProg.htm.

[2] J.A. Holmes, S. Cousineau, V.V. Danilov, S. Henderson, A. Shishlo, Y. Sato, W. Chou, L. Michelotti, and F. Ostiguy, *in The ICFA Beam Dynamics Newsletter*, Vol. 30, 2003.

[3] M.A. Plum, "SNS Injection and Extraction Systems Issues and Solutions," in *Proceedings of the 42nd ICFA Advanced Beam Dynamics Workshop on High-Intensity, High-Brightness Hadron Beams (HB2008)*, Nashville, August, 2008, http://neutrons.ornl.gov/workshops/hb2008/index.shtml.

[4] J.D. Jackson, "Classical Electrodynamics," Wiley, (New York: 1967).

[5] A. V. Fedotov and G. Parzen, in *Proceedings of the 2003 Particle Accelerator Conference*, Portland, May 2003, http://accelconf.web.cern.ch/AccelConf/p03/PAPERS/WPPG001.PDF.

[6] S. C. Bunch and J. Holmes, *U.S. Department of Energy Journal of Undergraduate Research* **IV**, (2004), 27.

[7] D. Sagan and D. Rubin, Phys. Rev. Special Topics - Accelerators and Beams **2**, (1999) 074001, http://prst-ab.aps.org/pdf/PRSTAB/v2/i7/e074001.

[8] J. Galambos, V. Danilov, J. Holmes, D. Jeon, F. Neri, D. K. Olsen, and M. Plum, Phys. Rev. Special Topics - Accelerators and Beams **3**, (2000) 034201, http://prst-ab.aps.org/pdf/PRSTAB/v3/i3/e034201.

[9] S. Cousineau, J. Holmes, J. Galambos, A. Fedotov, J. Wei, and R. Macek, Phys. Rev. Special Topics - Accelerators and Beams **6**, (2003) 074202, http://prst-ab.aps.org/pdf/PRSTAB/v6/i7/e074202.

[10] V. Danilov, S. Cousineau, A. Aleksandrov, S. Assadi, W. Blokland, C. Deibele, S. Henderson, J. Holmes, M. Plum, and A. Shishlo, "Accumulation of High Intensity Beam and Observations of First Instabilities in the SNS Accumulator Ring," in *Proceedings of the 41st ICFA Advanced Beam Dynamics Workshop on High-Intensity, High-Brightness Hadron Beams (HB2006)*, Tsukuba, Japan, May, 2006, http://accelconf.web.cern.ch/AccelConf/abdwhb06/PAPERS/TUAX01.PDF.

[11] S. Cousineau, "Instability Observations in the SNS Accumulator Ring," in *Proceedings of the 42nd ICFA Advanced Beam Dynamics Workshop on High-Intensity, High-Brightness Hadron Beams (HB2008)*, Nashville, August, 2008, http://neutrons.ornl.gov/workshops/hb2008/index.shtml.

[12] J. Holmes, V. Danilov, and L. Jain, "Transverse Stability Studies of the SNS Ring," in Proceedings of the 2005 Particle Accelerator Conference, Knoxville, 2005, http://accelconf.web.cern.ch/AccelConf/p05/PAPERS/TPAT032.PDF.

[13] A. Shishlo, S. Cousineau, V. Danilov, S. Henderson, J. Holmes, M. Plum, "Electron Cloud Self-Consistent Simulation for the SNS Ring," EPAC'06, Edinburgh, (2006); http://accelconf.web.cern.ch/AccelConf/e06/PAPERS/THPCH025.PDF.